Biological Applications of Size-Controlled Iron Oxide Magnetic Nanostructures

Student Researchers
Seul Kathy Ku, Maine East High School, Park Ridge, IL
Jonathan Lin, Northwestern University, Evanston, IL

Faculty Mentor
Vinayak P. Dravid
Department of Materials Science and Engineering
Northwestern University

Postdoctoral Mentor
Hrushikesh M. Joshi
Department of Materials Science and Engineering
Northwestern University

Abstract

Magnetic nanostructures (MNS) have become the subject of intense interest due to their superparamagnetic properties and consequently their potential uses in medical diagnostics and therapeutics. In this study, monodisperse magnetite MNSs were synthesized via thermal decomposition of iron(III) acetylacetonate and transferred to aqueous solution using 11-aminoundecanoic acid as the surfactant. Fluoroscein isothiocyanate (FITC) was then conjugated to the MNSs for the purposes of tracking the MNSs in vitro and identifying amine functional groups available on the surface of the nanostructures. Synthesis and proper conjugation of the FITC-functionalized MNSs were verified using transmission electron microscopy (TEM), Fourier transform infrared spectroscopy (FTIR), and UV/vis spectroscopy. The biocompatibility of the FITC-functionalized MNSs was demonstrated by incubating HeLa cells with the MNSs. MNS uptake by the cells was verified using confocal fluorescent microscopy, and cytotoxicity was determined by performing a viability assay. The identification of amine groups on the surface of a biocompatible nanostructure known to be coated in carboxylic acid groups opens the door to the development of multifunctionalized nanostructures for biomedical diagnostics and therapeutics.

Introduction

At the core of the interest in MNSs is the phenomenon of superparamagnetism. Unlike conventional magnets, which lose their magnetic properties above their Curie point, a superparamagnetic material possesses paramagnetic properties below its Curie point —meaning that it can be magnetized by an external magnetic field but loses its magnetization when the external field is removed.[1] This demagnetization occurs because there is sufficient energy at the nanometer scale — even when thermal energy is insufficient to knock magnetic dipoles out of alignment — to change the magnetic moment of particles.

Because of their magnetic and superparamagnetic properties, MNSs have many potential applications in medical diagnostics and therapies. In previous research, MNSs have been shown to enhance contrast in magnetic resonance imaging (MRI) and, due to their ability to absorb energy from alternating magnetic fields,[2–4] have demonstrated promise as thermal activation therapy agents for diseases such as cancer.

The synthesis of magnetite (Fe_3O_4) MNSs has been the basis of many studies, each proposing different synthesis methods yielding nanostructures of different properties.[1] While there are many advantages to MNSs, including their low toxicity, the difficulty in synthesizing high-quality particles that can be used in biological studies is a great barrier.[4–7] Previous studies have aimed to create particles that are synthesized in organic phase, but these particles have limited biological applications due to the toxicity of organic solvents.[1,8] There are, therefore, two difficulties: in synthesizing nanostructures with desirable properties and in producing particles that are compatible with biological systems.

In this study, biologically compatible Fe_3O_4 nanostructures were synthesized in order to explore their potential use in biomedical applications. The physical and magnetic properties of these nanostructures were examined to determine their possible applications in MRI contrast enhancement and thermal activation therapy. Also, the nanostructures' chemical properties were examined to determine means by which functional molecules such as fluorophores and biorecognition molecules can be conjugated to the nanostructures. In addition, the researchers determined the cytotoxicity of the nanostructures and observed some of the interactions of the nanostructures with biological systems. Characterizing these nanostructures and demonstrating their potential uses pave the way to the development of smart MNSs for targeted diagnostics and therapeutics of human diseases, including cancer and Alzheimer's disease.

Background

Synthesis of Magnetite MNSs

Many studies have demonstrated methods by which monodisperse magnetic iron oxide nanostructures may be synthesized, and here a modification of a method developed by Sun et al. was used, substituting lauric acid and dodecylamine for oleic acid and oleylamine.[8] Monodispersity is of particular interest because magnetic properties of MNSs are highly dependent on structure size and geometry.[1] Monodispersity is critical to obtaining particles with uniform and consistent properties.

Ligand exchange for the purpose of transferring MNSs from organic to aqueous phase has also been documented in previous studies. Here, a method similar to that developed by Sun et al. was employed, using 11-aminoundecanoic acid as the ligand.[8] In previous research, Sun et al. showed that when a similar surfactant, tetramethylammonium 11-aminoundecanate, was used, the amine functional group is bound to the nanostructure surface, leaving the carboxylic acid free.[8] Detecting the presence of free amine groups, in addition to the documented

carboxylic acid groups, on the surface of the nanostructures was a primary goal of this research. The detection of two functional groups on the surface of the nanostructures is of particular interest because several methods of conjugating biological molecules and other functional molecules to both amine and carboxylic acid functional groups have been demonstrated in previous studies. With both functional groups present, it may be possible to synthesize multifunctionalized particles that will aid in targeting and detecting the nanostructures in vitro.

MRI Contrast Enhancement

In the past few decades, MRI has become a commonplace medical diagnostic tool. MRI functions by generating a magnetic field to which hydrogen protons align. Once aligned, these protons are knocked out of alignment by a transverse radiofrequency pulse and then observed as they return to their initial alignment, a process known as relaxation. Relaxation times measured by the MRI machine are used to render an image of the human body.

There remains much room for improvement of MRI technology. For instance, MR images often lack sufficient image contrast, requiring the use of injectable or ingestible contrast agents to aid in the identification of diseased tissue. Current commercial contrast agents, which have the problem of low signal transmittance,[9] can be replaced by superparamagnetic Fe_3O_4 nanostructures. The latter can be controlled by an outside magnetic field, making them the optimum agent for biological delivery and therapeutic purposes.

Magnetite MNSs are of particular interest for a number of reasons. First, iron oxide nanostructures have been found to be metabolized normally by human cells, so they can be used safely without significant side effects — unlike conventional Gadolinium-based contrast agents, which have shown signs of toxicity. Several products already approved by the FDA use iron oxide MNSs to enhance contrast in MR imaging. Second, the superparamagnetic properties of magnetite nanostructures allow magnetite MNSs to act as transverse relaxation (T_2) contrast agents, darkening MR images by decreasing the T_2 of nearby protons.[1] Thus, cells or tumors surrounded by magnetite MNSs appear brighter than their surroundings, making for easier diagnosis. It is important to note that since particles' magnetic properties can change based on particle size, iron oxide nanostructures must be nearly monodisperse in size and shape to provide uniform magnetic properties. Fortunately, great control over size and geometry[1,8,10,11] is now possible in the creation of monodisperse iron oxide nanostructures.

Iron oxide nanostructures are stable in cells at MRI-detectable levels for up to six days after initial exposure.[4] The ability of the particles to continue offering MRI contrast for a period of time opens up many possibilities, such as improved postoperative monitoring of patients.

Thermal Activation

Another interesting phenomenon that results from superparamagnetism is that superparamagnetic particles can be heated using high-frequency, alternating magnetic fields. Although the exact contribution of different physical phenomena to particle heating is still being investigated, it has been shown that at a nanometer scale, Néel relaxation (i.e., mean time between two reversals of magnetic direction) contributes significantly to the thermal activation of magnetic particles. The temperature increase of superparamagnetic nanostructures resulting from Néel losses is dependent on numerous variables, ranging from particle size to strength and frequency of the alternating magnetic field. While increasing field strength and frequency generally improves the rate of temperature increase, increase in particle size improves the rate of temperature increase to a threshold after which the rate begins to decrease.[12]

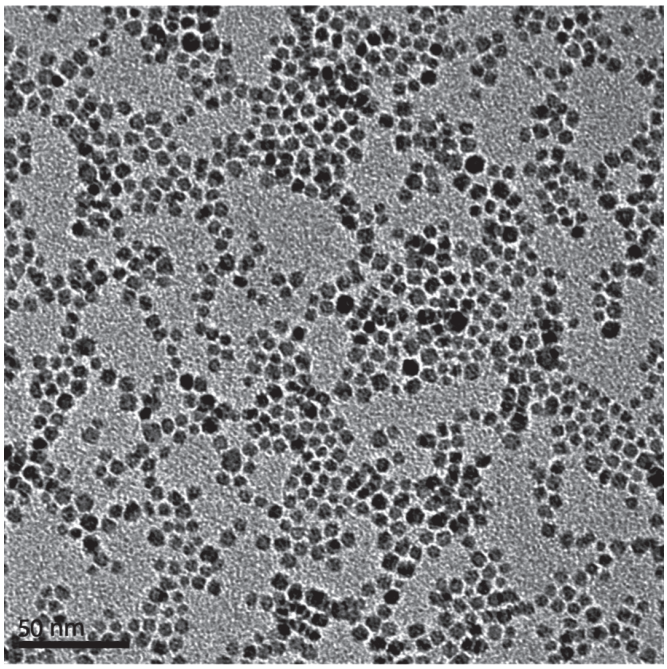

Figure 1. TEM of MNS in hexane. Note the size scale and that the particles are relatively monodisperse.

The ability to thermally activate superparamagnetic iron oxide nanostructures can be exploited as a therapy for diseases such as cancer. It has been shown that cancer cells are highly sensitive to temperature, and that temperatures between 42° and 46° C can lead to apoptosis.[13,14] Thus, since their heat-generation abilities have been demonstrated several times (Gordon et al. measured a 8° C/min rise in temperature using ferrofluid of dextran magnetite under a 450 kHz, 38 kA/m AC magnetic field), iron oxide nanostructures can be delivered to cancer cells and activated ex vivo, causing cancer cells to apoptosize.[15] Much work has been done with direct injection into tumors and other, more precise methods of targeting, such as the use of antibodies,[16–19] but no method of specifically targeting cancer cells in vivo has yet been developed.

Approach

Synthesis of Iron Oxide Nanostructures

To study the use of magnetic iron oxide nanostructures, 6–8 nm particles were synthesized via the thermodecomposition of Fe(III) acetylacetonate as performed by Sun et al.: $Fe(acac)_3$ (2 mmol), 1,2-hexadecanediol (10 mmol), lauric acid (6 mmol) and dodecylamine (6 mmol) were dispersed in benzyl ether (20 mL). The resulting mixture was placed under nitrogen and held at 200° and 285° C for 30 min, with the temperature of the solution increased 2–3° C per minute. The viscous solution was then cooled to room temperature and treated with ethanol and acetone to precipitate. After the supernatant was removed, the particles were resuspended in hexane. The purification process using

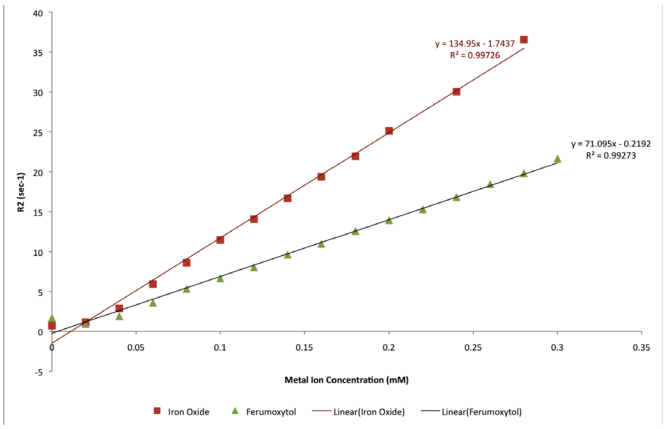

Figure 2. MRI of magnetite MNS and ferumoxytol. Note that the slope of the magnetite MNS line is larger than that of ferumoxytol.

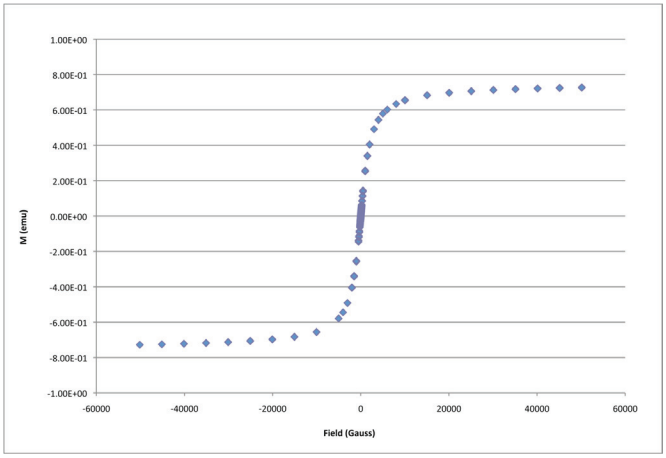

Figure 3. SQUID data for magnetite MNSs. Note the absence of a hysteresis loop, indicating that the nanostructures lack magnetic remanence and are superparamagnetic.

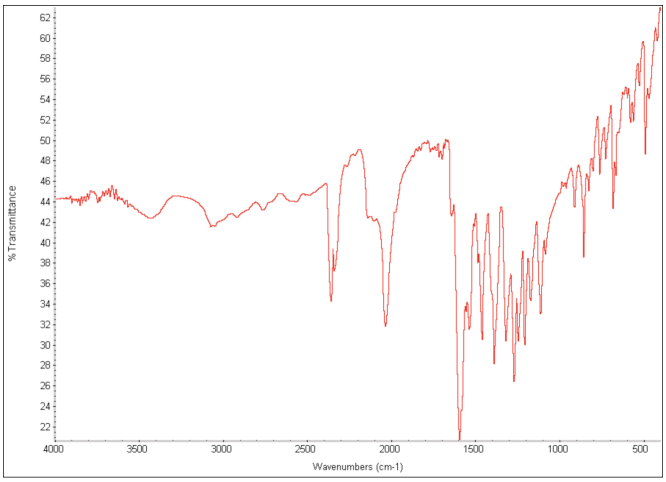

Figure 4. IR Spectrum of FITC. Note the broad peak at 2,100 wavenumbers, which corresponds to the isothiocyanate group of FITC.

ethanol, acetone, and hexane was repeated twice more to ensure that no excess organic solutes remained in the solution. TEM was then performed using a Hitachi HD 8100 TEM.

Phase Transfer of NPs

Because in their organic phase they cannot be used for biological studies without damaging biological samples, the nanostructures were dried by evaporating the hexane solution at room temperature. The MNSs were then transferred to aqueous phase via ligand exchange, using the ligand 11-aminoundecanoic acid. The ligand exchange was performed by dissolving 11-aminoundecanoic acid in ethanol. The ligand solution was then combined with an equivalent mass of MNSs dissolved in hexane and left overnight. The MNSs were then separated from solution using a magnet and washed three times with ethanol before being dispersed in water.

Magnetic Measurements Using MRI and SQUID

In order to quantify the efficacy of the nanostructures as an MRI contrast agent, the relaxivity coefficient was determined using MRI. After the concentration of the MNS solution was determined to be 3.5 mg/mL using ICP-AES, the solution was serially diluted to form solutions between 0 and 0.3 mM by increments of 0.02 mM. Three samples of every concentration were created to ensure uniformity in measurement, and the spin-spin relaxation time, or T_2, was measured for each sample using a Siemens 2.0 Tesla MRI scanner.

To ensure that the efficacy of iron oxide MNPs exceeds that of existing commercial contrast agents, the T_2 spin-spin relaxation time of the particles was compared with that of ferumoxytol, a commercial iron oxide contrast agent.

To confirm the superparamagnetism of the iron oxide particles, superconducting quantum interference device (SQUID) measurements were taken. To prepare samples for SQUID, MNSs were dried by allowing their hexane solvent to evaporate at room temperature. SQUID was performed on 32.6 mg of the resultant powder. The data were then analyzed for evidence of magnetic remanence.

Toxicity of MNPs

The biocompatibility of the nanostructures was determined by incubating HeLa cells with iron oxide nanostructures suspended in 10% FBS MEM media (iron concentrations ranged between 0 and 3.5 mg/mL). HeLa cells were incubated in the suspensions for 24 hr. The cells were then treated with Guava ViaCount reagent according to manufacturer instructions to determine whether the particles caused cell death.

FITC Conjugation and Nanostructure Internalization

To determine if amine groups were present on the outer surface of the MNSs, the nanostructures were tagged with fluorescein isothiocyanate (FITC). The isothiocyanate group reacts specifically with primary amines; consequently, successful conjugation with the MNSs would indicate the presence of amine functional groups on the nanostructure surface. Conjugation was performed by dissolving 2 mg of FITC in 200 mL of dimethylsulfoxide. This solution was combined with 4 mL of MNS suspension and left overnight. It was then dialyzed for 24 hr in deionized water. The nanostructures were then dried and formed into a KBr pellet for analysis using FTIR. Unconjugated FITC was compared with the MNS-FITC conjugates. Confirmation of conjugation was performed using UV/vis spectroscopy in which MNS-FITC conjugates were compared against unconjugated MNSs and FITC.

With FITC-conjugated MNSs, the researchers confirmed the internalization of nanostructures by HeLa cells. After the cells were treated with the particles for 24 hr, nuclear staining was performed using 4',6-diamidino-2-phenylindole (DAPI). The cells were then immediately imaged using a Zeiss dual-photon confocal inverted microscope. A Z-stack analysis was performed to confirm nanostructure internalization.

Results

Following the organic phase synthesis of the MNSs, a TEM image was taken of the nanostructures, confirming that they were monodisperse spheres, 6–8 nm in diameter (Figure 1). Next, the nanostructures were transferred from hexane into water via ligand exchange. Prior to the ligand exchange, the nanostructures were dispersible in hexane but not in water. Following the exchange, the nanostructures were dispersible in water but not in hexane. The resultant aqueous suspension contained no visible aggregates and was a solid brown-black color.

Following size and geometry verification and phase transfer, SQUID and MRI were performed on the particles to verify their magnetic properties. As shown in Figure 2, the relaxivity coefficient of the iron oxide nanoparticles was 134.95 mM^{-1} sec^{-1}, compared with 58.609 mM^{-1} sec^{-1} for ferumoxytol. The calculation was performed by graphing the spin-spin relaxation time of the agents with respect to concentration. The slope of a linear regression model fit to the data represents the relaxivity coefficient of the agents. The data collected using SQUID showed the absence of a hysteresis loop, indicating that the nanostructures lacked magnetic remanence and were consequently superparamagnetic (Figure 3).

In order to detect the presence of free primary amines, the nanostructures were conjugated with FITC. After conjugation and dialysis, the suspension appeared noticeably more yellow than the suspension prior to conjugation. FTIR was then used to confirm proper conjugation. Looking at the IR spectrum of FITC (Figure 4), the researchers observed a broad peak around 2,100 wavenumbers, which corresponds to the C=N and C=S vibrations of the isothiocyanate group. In the IR spectrum of the MNS-FITC conjugates (Figure 5), the broad peak near 2,100 wavenumbers was absent.

Following IR spectroscopy, UV/vis spectroscopy was performed to further confirm FITC conjugation (Figure 6). Note that both the FITC and the MNS-FITC conjugates had a broad absorption peak around 450 nm, but unfunctionalized MNSs did not.

As for the biocompatibility of the nanoparticles, ViaCount showed that various concentrations of magnetite particles were nontoxic to the cells, as shown in Figure 7. Regardless of the concentration, more than 90% of the HeLa cells were still viable after 24 hr. Following a 24-hr incubation time, HeLa cells incubated with particles of 13.8 mg/L iron concentration conjugated with FITC were imaged. The confocal image in Figure 8 shows the overlap of DAPI and FITC-tagged particles. Figure 9 confirms that the DAPI and FITC are on the same plane, indicating that the particles were internalized through passive uptake rather than remaining near the membrane.

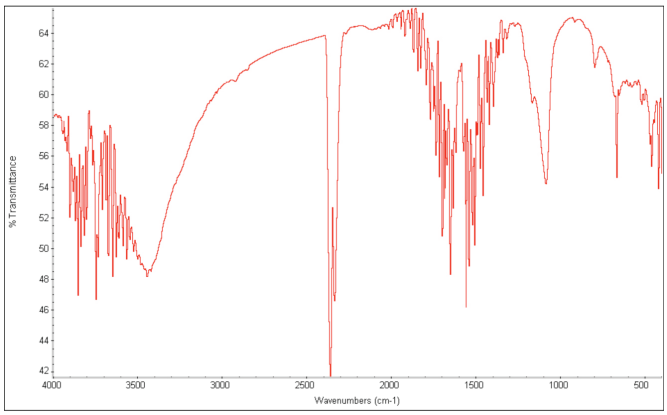

Figure 5. IR Spectrum of MNS-FITC conjugates. Note that the broad peak at 2,100 wavenumbers is not present in this sample.

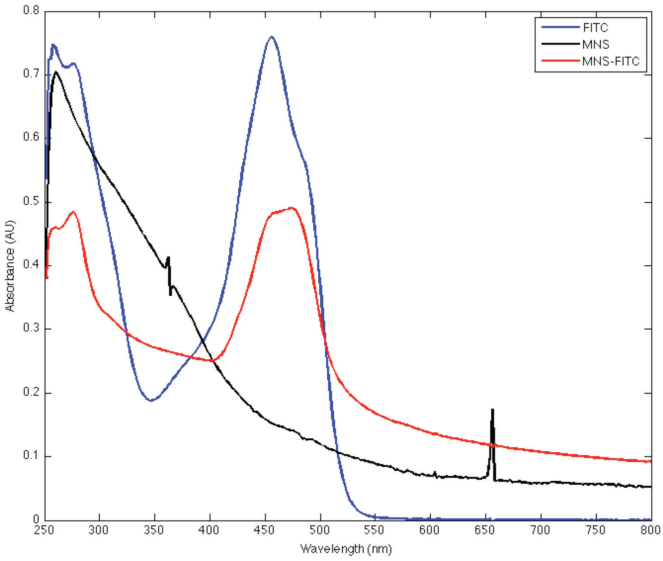

Figure 6. UV/vis spectra of MNS, FITC, and MNS-FITC conjugates. Note that both the MNS-FITC conjugates and FITC have wide absorption peaks at ~450 nm.

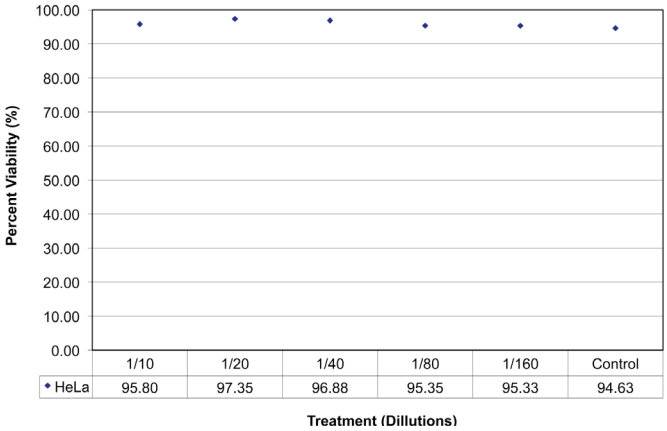

Figure 7. ViaCount results for HeLa cells incubated for 24 hr with magnetite MNSs.

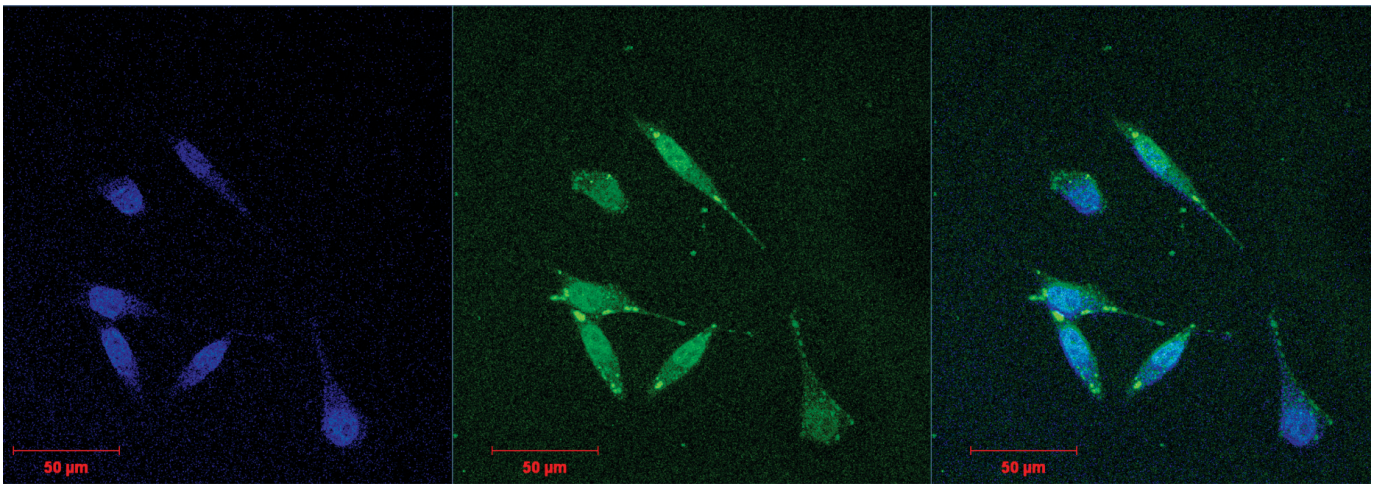

Figure 8. Confocal fluorescence image of HeLa cells incubated with FITC-tagged magnetite MNSs. Note how the nuclear DNA stain, DAPI (blue), colocalizes with the FITC (green), indicating that the MNSs were internalized by the cells.

Discussion

The TEM image in Figure 1 suggests that the synthesis was successful. The particles appear relatively monodisperse and spherical, ranging from 6 to 8 nm in diameter. Following the phase transfer, the MNSs appeared completely suspended in solution, and the liquid was a solid black-brown color with no visible aggregates, indicating that the ligand exchange was successful. Even after the solution was left for several days, no aggregation was observed, further indicating that ligand exchange was successful.

MRI performed on the nanostructures showed that they have a higher relaxivity coefficient (134.95 $mM^{-1}sec^{-1}$) than does the commercially available ferumoxytol (58.609 mM^{-1} sec^{-1}), indicating that the nanostructures are a viable contrast agent (Figure 2). Furthermore, the data obtained from SQUID in Figure 3 lack a hysteresis loop; although the nanostructures became magnetized in the presence of a magnetic field, they had no magnetic remanence when the magnetic field was removed, making them suitable for biological applications.

The FTIR and UV/vis data in Figures 4–6 indicate that FITC conjugation occurred successfully. The disappearance of the broad peak at 2,100 wavenumbers in the MNS-FITC conjugate spectra indicates that either the isothiocyanate group reacted with primary amines on the nanostructure surface or that FITC was lost during the washing process. Looking at the UV/vis data, however, it appears that the FITC was bound to the particle surface, since the MNS-FITC conjugates absorbed at the same wavelengths as unbound FITC. Thus, the conjugation of FITC to the particle surface as well as the presence of primary amines on the nanostructures surface were confirmed.

Data from the biocompatibility study indicated that the nanostructures were largely nontoxic at even high concentrations, further confirming that MNSs are suitable for biological applications (Figure 7). Furthermore, the MNS-FITC conjugates, when incubated with HeLa cells, were readily absorbed into the cells, as was shown using Z-stack confocal microscopy (Figure 9). This finding has important implications: Not only does it show that the particles were nontoxic when internalized, it also shows that thermal activation therapy may be a viable therapeutic option when MNSs can be introduced at the site of diseased tissue.

Conclusions

The results from this study indicate that it is not only possible but also relatively simple to synthesize biologically compatible iron oxide nanostructures. The ability to generate monodisperse particles that can be transferred to aqueous phase means that it is possible to develop nanostructures with consistent properties that can be used in biomedical applications. In addition, it was observed that these nanostructures are superparamagnetic and have strong MRI contrast-enhancing capabilities.

The success of FITC conjugation demonstrated the flexibility of these MNSs. FITC allows researchers to track the position of the MNSs in vitro, allowing future research to examine the interaction of MNSs with biological systems. Furthermore, the successful FITC conjugation, along with the assertion by Sun et al. that carboxylic acids dominate nanostructures using 11-aminoundecanoic acid as the surfactant, indicated that two different functional groups were present on the particle surface, allowing for the addition of at least two different types of functional molecules. Consequently, these nanostructures can be used to create multifunctional nanostructures, such as ones bearing both biorecognition molecules and molecular tags. Such multifunctional nanostructures can allow researchers to create diverse, versatile nanostructures and examine the possibilities of using the nanostructures for diagnostics and therapeutics.

The biological experiments included in this study indicate that the nanostructures are nontoxic, even at high concentrations and when absorbed by the cells. Furthermore, because the nanostructures were absorbed by the cells, they may be able to be used in thermal activation therapy as well as in the magnetically driven movement of cells.

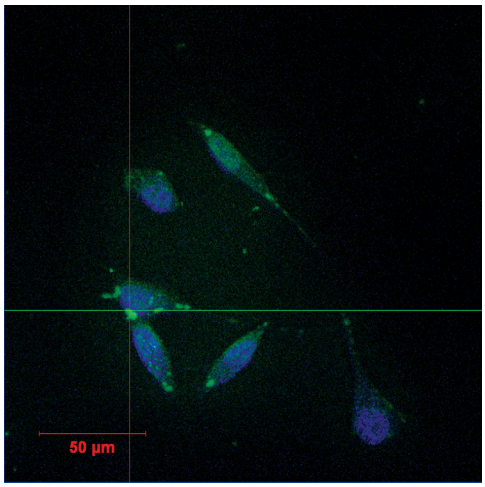

Figure 9. Confocal image of HeLa cells incubated with FITC-labeled magnetite MNS. Note that FITC and DAPI appear on the same plane, indicating that the nanostructures were internalized by the cells.

Future experiments would include growing the nanostructures to larger sizes so that they are better able to absorb energy during thermal activation therapy. Also, different doping agents, such as manganese and cobalt, have shown promise in enhancing the magnetic properties of iron oxide MNSs. These doping agents deserve further attention.

In summary, this study demonstrated the flexibility and wide applicability of iron oxide nanostructures. Both superparamagnetic and biocompatible, these nanostructures can be used in the development of potent MRI contrast agents and thermal therapeutic agents. These abilities, coupled with the ability to multifunctionalize the surface of the nanostructures, make iron oxide nanostructures ideal for the development of a targeted diagnostic and therapeutic package.

This research was supported primarily by the Center of Cancer Nanotechnology Excellence (CCNE) initiative of the National Institutes of Health (NIH) under award number ***U54 – CA119341*** *(Lin) and through the American Recovery and Reinvestment Act of 2009 under award number* ***U54 – CA119341*** *(Ku). Any opinions, findings, conclusions or recommendations expressed in this material are those of the author(s) and do not necessarily reflect those of the NIH.*

References

1 Sun, C.; Lee, J. S. H.; Zhang, M. *Adv. Drug Deliv. Rev.* **2008,** *60,* 1252–1265.
2 Jun, Y. W.; Huh, Y. M.; Choi, J. S.; Lee, J. H.; Song, H. T.; Kim, S.; Yoon, S.; Kim, K. S.; Shin, J. S.; Suh, J. S.; Cheon, J. *J. Am. Chem. Soc.* **2005,** *127,* 5732–5733.
3 Weissleder, R.; Bogdanov, A.; Neuwelt, E. A.; Papisov, M. *Adv. Drug Deliv. Rev.* **1995,** *16,* 321–334.
4 Sun, R.; Dittrich, J.; Le-Huu, M.; Mueller, M. M.; Bedke, J.; Kartenbeck, J.; Lehmann, W. D.; Krueger, R.; Bock, M.; Huss, R.; Seliger, C.; Grone, H. J.; Misselwitz, B.; Semmler, W.; Kiessling, F. *Invest. Radiol.* **2005,** *40,* 504–513.
5 Weissleder, R.; Stark, D. D.; Engelstad, B. L.; Bacon, B. R.; Compton, C. C.; White, D. L.; Jacobs, P.; Lewis, J. *Am. J. Roentgenol.* **1989,** *152,* 167–173.
6 Paunesku, T.; Vogt, S.; Lai, B.; Maser, J.; Stojicevic, N.; Thurn, K. T.; Osipo, C.; Liu, H.; Legnini, D.; Wang, Z.; Lee, C.; Woloschak, G. E. *Nano. Lett.* **2007,** *7,* 596–601.
7 Kim, D. K. Z., Y.; Kehr, J.; Klason, T.; Bjelke, B.; Muhammed, M. *J. Magn. Magn. Mater.* **2001,** *225,* 256.
8 Sun, S. H.; Zeng, H.; Robinson, D. B.; Raoux, S.; Rice, P. M.; Wang, S. X.; Li, G. X. *J. Am. Chem. Soc.* **2004,** *126,* 273–279.
9 Jun, Y.-w.; Huh, Y.-M.; Choi, J.-s.; Lee, J.-H.; Song, H.-T.; KimKim; Yoon, S.; Kim, K.-S.; Shin, J.-S.; Suh, J.-S.; Cheon, J. *J. Am. Chem. Soc.* **2005,** *127,* 5732–5733.
10 Kang, E.; Park, J.; Hwang, Y.; Kang, M.; Park, J. G.; Hyeon, T. *J. Phys. Chem. B* **2004,** *108,* 13932–13935.
11 Sun, S. H.; Zeng, H. *J. Am. Chem. Soc.* **2002,** *124,* 8204–8205.
12 Hergt, R.; Andra, W.; d'Ambly, C. G.; Hilger, I.; Kaiser, W. A.; Richter, U.; Schmidt, H. G. *IEEE Trans. Magn.* **1998,** *34,* 3745–3754.
13 Overgaard, J. *Cancer* **1977,** *39,* 2637–2646.
14 Overgaard, K; Overgaard, J. *Eur. J. Cancer* **1972,** *8,* 65.
15 Gordon, R. T.; Hines, J. R.; Gordon, D. *Medical Hypotheses* **1979,** *5,* 83–102.
16 Le, B.; Shinkai, M.; Kitade, T.; Honda, H.; Yoshida, J.; Wakabayashi, T.; Kobayashi, T. *J. Chem. Eng. Jpn.* **2001,** *34,* 66–72.
17 Weissleder, R.; Lee, A. S.; Fischman, A. J.; Reimer, P.; Shen, T.; Wilkinson, R.; Callahan, R. J.; Brady, T. J. *Radiology* **1991,** *181,* 245–249.
18 Tiefenauer, L. X.; Kuhne, G.; Andres, R. Y. *Bioconj. Chem.* **1993,** *4,* 347–352.
19 Bulte, J. W. M.; Hoekstra, Y.; Kamman, R. L.; Magin, R. L.; Webb, A. G.; Briggs, R. W.; Go, K. G.; Hulstaert, C. E.; Miltenyi, S.; The, T. H.; Deleij, L. *Magn. Reson. Med.* **1992,** *25,* 148–157.